JOURNAL OF THERMOPHYSICS AND HEAT TRANSFER
Vol. 11, No. 3, July–September 1997

Survey of Blunt Body Flows Including Wakes at Hypersonic Low-Density Conditions

James N. Moss and Joseph M. Price
NASA Langley Research Center, Hampton, Virginia 23681

Nomenclature

A = base area of cone, $\pi d^2/4$
a = acceleration
C_D = drag coefficient, $2D/\rho_\infty V_\infty^2 A$
C_H = heat transfer coefficient, $2q/\rho_\infty V_\infty^3$
$\overline{C_H}$ = overall heat transfer coefficient, $2Q/\rho_\infty V_\infty^3 A$
C_p = modified pressure coefficient, $2p_w/\rho_\infty V_\infty^2$
D = drag
d = base diameter
Kn = Knudsen number, λ/d
M = Mach number
n = number density
p = pressure
Q = overall (integrated) heat transfer
q = heat transfer rate
R_b = cone base radius
R_c = corner radius
Re_∞ = Reynolds number, $\rho_\infty V_\infty d/\mu_\infty$
R_f = filet radius, between base and sting
R_n = nose radius
R_s = sting radius
s = distance along the body surface measured from the stagnation point
T = temperature
u = axial velocity
V = freestream velocity
x = axial distance from stagnation point measured along symmetry axis
y = radial distance from symmetry axis
λ = mean free path
μ = viscosity
ρ = density

Subscripts
w = surface values
0 = total or stagnation values
∞ = freestream values

Introduction

SINCE December 1991, the AGARD Fluid Dynamics Panel (FDP) has promoted[1] the activities of Working Group 18 (WG 18) to address a wide range of problems associated with hypersonic flows. One of the problems selected for investigation was the effect of rarefaction and real gas on blunt body wake flows. Interest in this particular problem arises from the complex flow features that evolve as the compressed forebody flow rapidly expands into the near wake. Flow features of importance for flight application include high-temperature effects (thermochemical nonequilibrium), rarefaction, separation, free shear layers, flow reattachment, and transition to turbulence at high Reynolds number conditions. Also of issue are the conditions for which the near-wake flow can become unsteady. Not only are these processes of fundamental importance, but also of practical importance for the design of planetary probes and aerobrake vehicles.

An objective of the WG 18 activity was to promote both experimental and computational studies such that the synergy would produce an enhanced understanding of the physical phenomena and a test of the computational capability to predict/model such phenomena. The blunt body wake problem was organized (see Ref. 1) as two subproblems: 1) continuum flows where the major emphasis would be on test conditions conducted in moderate to high enthalpy impulse facilities complemented with perfect gas wind-tunnel data and 2) rarefied flows with tests conducted in low-density wind tunnels, free-

James N. Moss is a Senior Research Engineer in the Aerothermodynamics Branch at the NASA Langley Research Center. He received his B.S. in Engineering Science from the Tennessee Polytechnic Institute in 1962, his M.S. in Aerospace Engineering from the University of Virginia in 1968, and his Ph.D. in Aerospace Engineering from the Virginia Polytechnic Institute and State University in 1972. He also received an M.S. in Engineering Administration in 1988 from George Washington University. The author joined NASA Langley Research Center in 1962, where his early research assignments dealt with thermal protection materials and the aerothermodynamics of atmospheric entry. His current research concerns rarefied flows. He is a recipient of the AIAA Thermophysics Award (1989) and is a Fellow of the AIAA.

Joseph M. Price is a Research Engineer at the NASA Langley Research Center in the Aerothermodynamics Branch. He received his B.S. in Mathematics from Millsaps College in 1964 and has done advanced graduate work at the University of Mississippi in Numerical Analysis and at the College of William and Mary in Computer Science. He joined NASA Langley Research Center in 1965. He was responsible for providing the translation of the meteorological data for the initial Space Shuttle flights to the Shuttle location for determination of the local trajectory. More recently, he has worked in computer graphics.

Presented as Paper 96-1803 at the AIAA 31st Thermophysics Conference, New Orleans, LA, June 17–20, 1996; received Sept. 12, 1996; revision received Feb. 17, 1997; accepted for publication Feb. 20, 1997.

jets, and high-enthalpy impulse facilities by testing at either low-pressure conditions or by using very small models. The latter subproblem is the focus of the present review complemented with high altitude generic flight conditions for making code-to-code comparisons.

The forebody configuration for all experimental and generic flight conditions was a spherically blunted 70-deg half-angle cone with an outer corner radius as shown in Fig. 1. The forebody configuration is the same as that for the Mars Pathfinder Probe launched in December 1996, onboard a Delta II rocket; Mars arrival is planned for July 1997. The test models were supported with either an afterbody sting or small wires. Figure 2 displays the test conditions in terms of rarefaction, as indicated by lines of constant $M_\infty/\sqrt{Re_\infty}$, where the characteristic dimension is the base diameter. The larger this parameter is, the more rarefied the flow. As indicated, experiments have been performed in five different hypersonic facilities: 1) SR3 is a low-density wind tunnel of the CNRS, Meudon, France; 2) V2G is a low-density wind tunnel of the DLR, Göttingen, Germany; 3) V3G is a freejet facility at the DLR, Göttingen, Germany; 4) HEG is a high enthalpy free piston shock tunnel located at the DLR, Göttingen, Germany; and 5) LENS is the Large Energy National Shock tunnel located at Calspan, Buffalo, New York. Results obtained with these five facilities for the common model (70-deg spherically blunted cone) configuration are given in Refs. 2–11.

Extensive calculations have been performed for the experimental test conditions using direct simulation Monte Carlo (DSMC) and Navier–Stokes (NS) solvers.[12–23] In addition, calculations have been reported for generic flight conditions for both Earth (Refs. 24–26) and Mars (Ref. 27) entry environments for the same forebody configuration with a base diameter of 2 m.

The purpose of this paper is to identify and summarize the extent of the experimental and computational database currently available, identify significant findings, and identify gaps or possible deficiencies in the current data.

Also presented are comparisons between aerothermodynamic data extracted from the Japanese Re-entry Experiment (OREX)[28,29] and computational findings[29–32] under rarefied conditions. The DSMC comparisons with both the WG 18 test cases and the OREX data provide a broad spectrum of flow conditions for establishing a level of credibility for both the computational and experimental results.

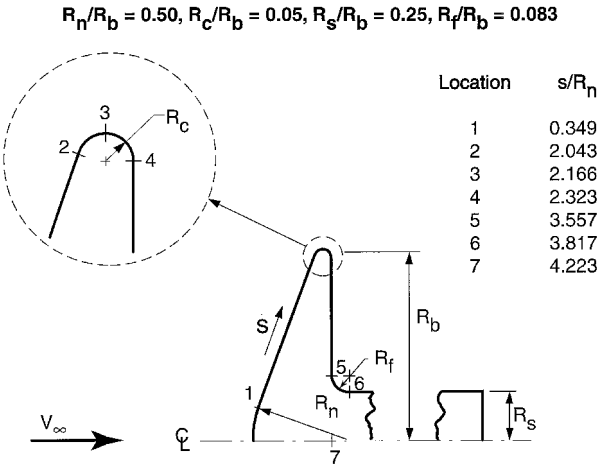

Fig. 1 70-deg spherically blunted cone configuration.

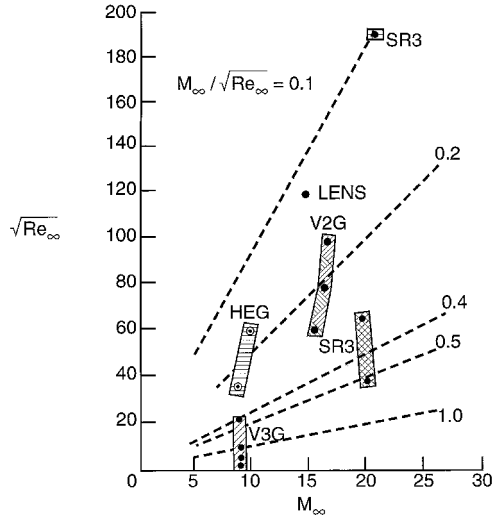

Fig. 2 Low-density test conditions in terms of the rarefaction parameter $M_\infty/\sqrt{Re_\infty}$.

Blunt Body/Wake Closure Experiments and Computations

A number of fundamental issues exist concerning wake flows at hypersonic conditions: how do the wake features change as a function of rarefaction; what role does thermochemical nonequilibrium play in the near wake; and to what limits are continuum models realistic as rarefaction in the wake is progressively increased. In an effort to address these issues, as part of the AGARD WG 18 activity, both experiments and computations have been performed for the same forebody configuration: a 70-deg spherically blunted cone with a nose radius equal to one-half the base radius and the corner or shoulder radius equal to 5% of the base radius (Fig. 1). Computations have been made for both wind-tunnel and flight conditions for the same forebody configuration. Results of experiments performed in each of the five hypersonic test facilities, along with some of the findings of the computational studies that have been made for specific test conditions, are briefly summarized.

The nominal test conditions for the low-density wind tunnels participating in the AGARD WG 18 investigation are listed in Table 1. Also included are the test conditions for two impulse facilities to achieve rarefied flow. One test was run in the LENS facility[10,11] at a low-pressure condition to produce Mach 15.6 nitrogen flow. Also, tests[7] were conducted in the HEG free piston shock tunnel using very small models (d = 5 mm). Two of the HEG test conditions in air are included in Table 1. Figure 2 displays these test conditions in terms of Reynolds and Mach numbers.

These test conditions provide a range of flow environments that include both nonreacting and reacting flows. Also, thermal nonequilibrium issues exist for even the lowest enthalpy tests (translational, rotational, etc.) with more internal modes participating for the higher enthalpy flows. Hence, the conditions include a variety of flow environments that serve as excellent test cases to measure the ability of numerical schemes to calculate such flows where compression, expansion, and separation are key features.

SR3 Results

Reference 2 provides a summary of the experiments conducted by the CNRS at Meudon, France, using the SR3 wind tunnel. Three test conditions (Table 1) were considered where the freestream was nitrogen at a nominal Mach number of 20 and Reynolds numbers, based on model base diameter, ranging from 1.42×10^3 to 3.6265×10^4. Measurements were performed that obtained three sets of data: density flowfields, heating rate distributions, and aerodynamic forces. Density flowfield measurements were made with the electron beam fluorescence technique for the two more rarefied conditions and for two angles of incidence: 0 and 10 deg. Heating rate distributions along the forebody, base, and sting, as well as aerodynamic forces, are presented for angle of incidence between 0–30 deg.

Table 1 Experimental test conditions

Test case	T_o, K	P_o, bar	M_∞	Re_∞/cm	$\rho_\infty \times 10^5$, kg/m^3	V_∞, m/s	T_∞, K	λ_∞,[a] mm	T_w, K	Gas
a) SR3 Wind tunnel, CNRS Meudon; d = 5 cm										
1	1100	3.5	20.2	285	1.73	1502	13.3	1.59	300	N_2
2	1100	10.0	20.0	838	5.19	1502	13.6	0.54	300	N_2
3	1300	120.0	20.5	7277	46.65	1633	15.3	0.06	300	N_2
b) V2G Wind tunnel, DLR Göttingen; d = 5, 2.5, and 0.5 cm										
1	575	2	15.6	719	6.70	1082	11.6	0.39	490	N_2
2	675	5	16.5	1233	11.02	1173	12.2	0.25	565	N_2
3	775	10	16.8	1935	17.25	1257	13.4	0.16	635	N_2
c) V3G Wind tunnel, DLR Göttingen, d = 0.5 cm										
1	295	0.163	9.0	859	14.22	759	17.2	0.16	Variable	N_2
2	295	0.0549	9.0	286	4.74	759	17.2	0.48	Variable	N_2
3	295	0.0163	9.0	86	1.42	759	17.2	1.60	Variable	N_2
4	295	0.0054	9.0	29	0.47	759	17.2	4.80	Variable	N_2
d) HEG, DLR Göttingen; d = 0.5 cm										
1	6713	576.0	10.1	7043	408.5	4539	489.9	0.017	300	Air
2	9244	385.0	9.5	2498	156.4	6075	856.4	0.044	300	Air
e) LENS, Calspan Buffalo; d = 15.24 cm										
1	4351	74.1	15.6	578	13.06	3246	103.7	0.35	294	N_2

[a]Evaluated with variable hard sphere model.

The test models utilized had the same external dimensions and were sting supported. The model base diameter was 5 cm; whereas the sting had a diameter of 1.25 cm and extended 7.5 cm downstream of the base plane before the sting cross-sectional area began to increase (see Ref. 1, Chap. 4, Fig. 9). Details concerning the models, instrumentation, test procedures, and tabulated and graphical presentations of results are given in Ref. 2.

A unique aspect of the SR3 tests was the density measurements that included flowfield values both with and without the model. The use of the nonintrusive electron beam fluorescence technique to provide measurements of the near wake and forebody density field provided the first such data for a generic aeroassist orbital transfer vehicle (AOTV) configuration.

Extensive computations have been made for the SR3 test conditions since the test parameters were defined well in advance of the actual experiments. Test condition 2 (Table 1) was a test case of the 4th European High-Velocity Database Workshop, ESTEC, Noordwijik, The Netherlands, Nov. 1994. Eight DSMC solutions were presented at this workshop and a summary of those results are given in Ref. 22.

Calculations using both DSMC and Navier–Stokes solvers were made either prior to the experiments (e.g., Refs. 12, 13, and 21–23) or prior to release of the experimental data at the ESTEC Workshop.[22] Reference 14 provides an extensive presentation of information concerning flowfield features and surface quantities (including tabulated surface results) resulting from one set of DSMC calculations. Also reported in Ref. 14 are the results of parametric studies concerning numerics (cell size and time step) and physical modeling (rotational collision number and surface reflection model).

Examples of the calculated and measured results for the SR3 tests are shown in Figs. 3–5. Examples of the surface heating distributions at zero incidence are presented in Fig. 3 for each of the three test conditions. As evident by the comparisons, the DSMC solutions[17] show a better agreement with the measured values than do the Navier–Stokes[33–36] methods (with surface slip and temperature jump boundary conditions) along the base plane and sting, regions where rarefaction effects are most significant. The agreement of DSMC predictions and measurements is quite good along the sting and also on the base plane, where measured signal levels for cases 1 and 2 were so small that the heating magnitude could only be characterized as being less than 0.002 and 0.004 W/cm^2, respectively (indicated by symbol with downward-pointing arrows in Fig. 3).

Along the forebody the agreement between calculated and measured results is not as good as expected.[17] Along the blunted cone forebody, agreement between calculation and measurement decreases with decreasing rarefaction. This is most evident for case 3 where the experimental value at s/R_n = 1.56 is 55% of the DSMC value. When the DSMC results along the forebody are compared with the Navier–Stokes solutions[17] the agreement is 10% or better. Currently, the discrepancy observed in measured and computed heat transfer distributions along the forebody remain unresolved. Further experiments are needed to resolve this issue.

Figure 4 presents the measured and calculated heat transfer distributions for case 2 with the model at incident angles of 0, 10, and 20 deg. The calculated values for both the windward and leeward rays are the three-dimensional DSMC solutions of Pallegoix.[23] Heat transfer measurements were made only along the windward ray where agreement with calculations is very good.

A number of computational studies have presented graphical results of the forebody and wake flow features, demonstrating the influence of rarefaction on the flow structure. The DSMC calculations of Refs. 12 and 14 yield a wake vortex for each of the three test conditions, with the size of the vortex increasing with decreasing rarefaction. Also, the location of maximum heating along the sting is downstream of the location of the free shear-layer reattachment, as indicated by the sting shear-stress distribution.

As mentioned earlier, nonintrusive electron beam fluorescence measurements of the flowfield density were made,[2] and Fig. 5 presents, as an example, a comparison of a DSMC calculation[17] with measured values. (See Ref. 22 for better agreement of computed and measured results and see Ref. 23 for good comparisons at 10-deg incidence.) The measured results are presented as the ratio of local density with the model installed in the test section of the wind tunnel to freestream values without the model in the test section, since density gradients exist in the undisturbed flow. The calculated results are

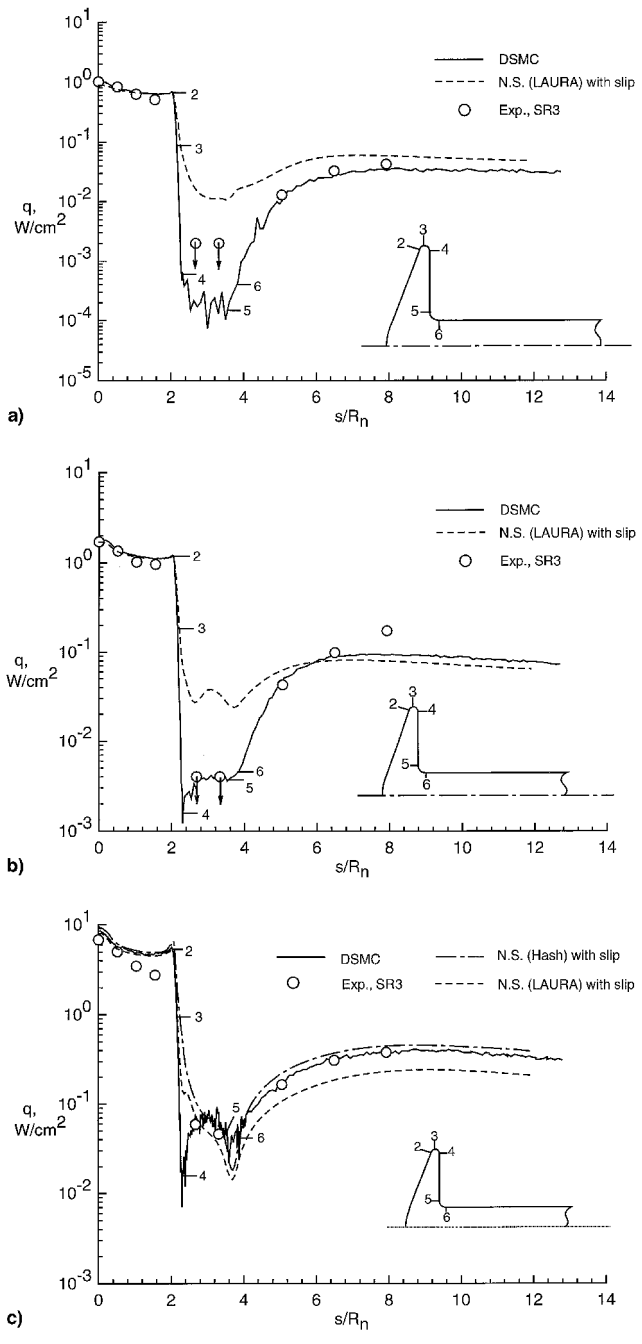

Fig. 3 Comparison of SR3 experimental[2] and computed[17] heating rate results (d = 5.0 cm). Case a) 1, b) 2, and c) 3.

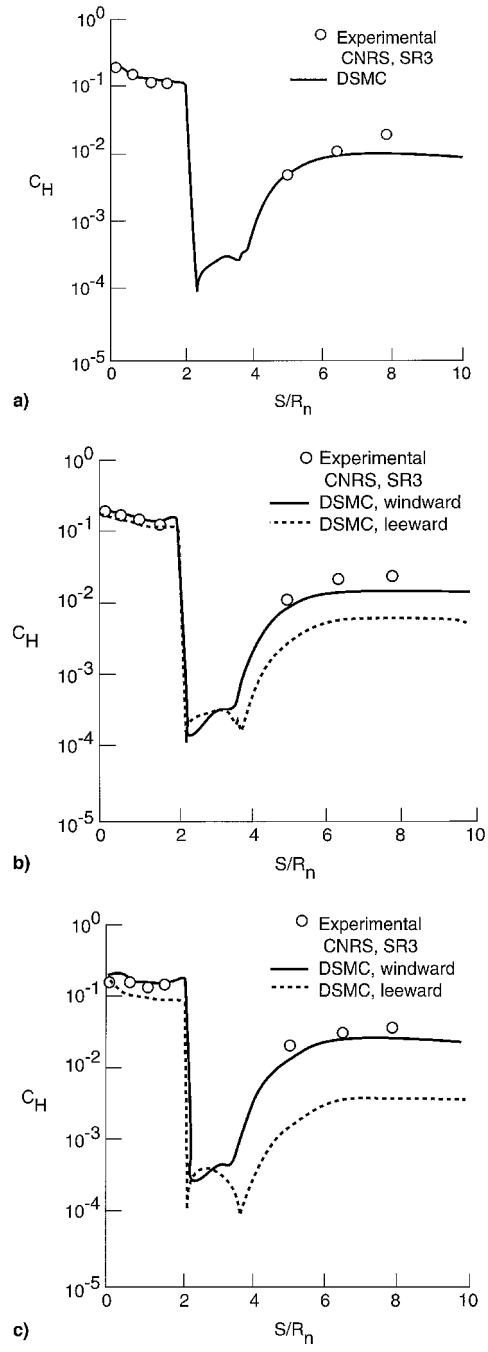

Fig. 4 Comparison of SR3 experimental[2] and computed[23] heating rate distributions for case 2. Incidence = a) 0, b) 10, and c) 20 deg.

local values ratioed to the freestream value (Table 1). The overall quantitative features of the two data sets are similar, with the exception of the expansion of the flow about the outer corner of the model and the sudden upturn of the 0.5 density contour adjacent to the sting. The calculated density contours in the near wake show a concentrated expansion from the rearward-facing portion of the outer corner. This behavior is consistent with other DSMC calculations that have been made for case 2, as summarized in Ref. 22, both at 0- and 10-deg incidence. The measurements show a more diffuse expansion extending down the base of the model. Part of this discrepancy may be due to a measurement resolution issue, since the gradients in density are substantial near the surface and occur in a rather small volume. As suggested in Ref. 22, the upturn of the measured density contours along the sting are most likely caused by an increase in the cross-sectional area of the sting starting 80.4 mm downstream of the forebody stagnation point of the model. The change in the sting configuration was not included in the numerical simulations; however, a numerical simulation accounting for the change in sting configuration, even if approximate, would be instructive.

The aerodynamic forces, moments, and c.p. were also measured for each flow condition at six angles of incidence spanning 0–30 deg. Tabulated results of these measurements are presented in Ref. 2. As reported in Ref. 17, the maximum difference in the measured and DSMC calculated drag coefficients for zero incidence was 6%. Reference 23 presents DSMC results for axial, normal, pitching moment, and c.p. results for case 2 flow conditions at 0-, 10-, and 20-deg incidence. The discrepancies with measured values are 11% or less.

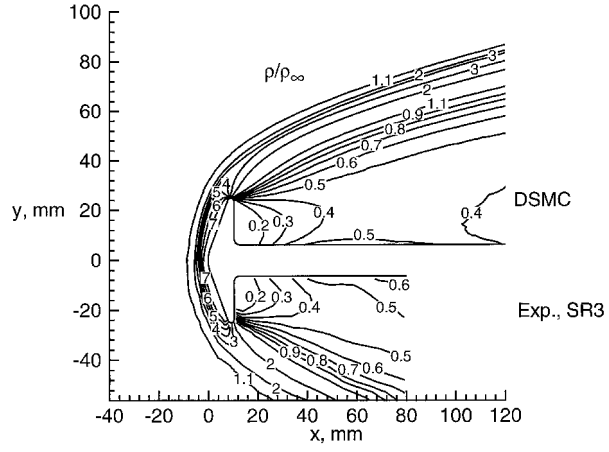

Fig. 5 Comparison of measured[2] and calculated[17] density for SR3 test case 2.

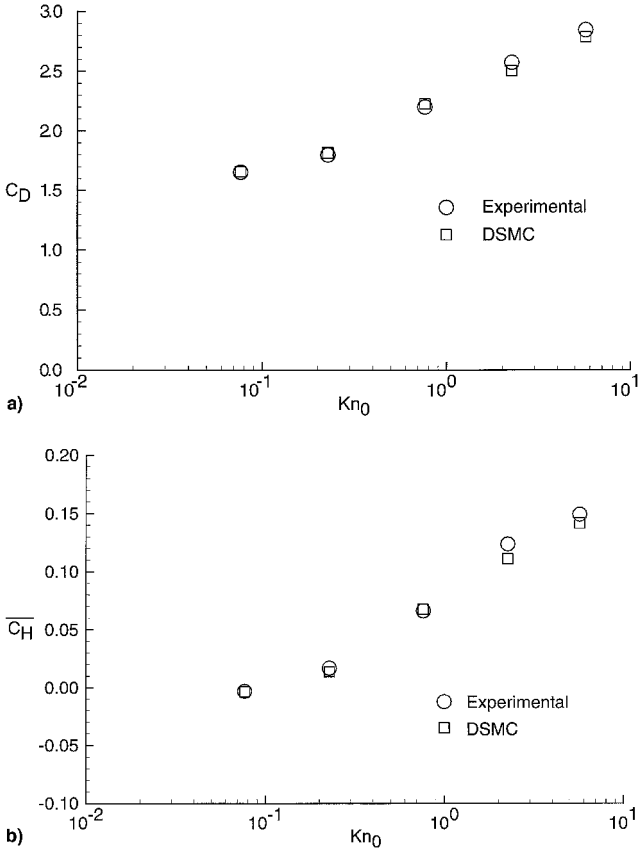

Fig. 6 Comparison of experimental[3] and DSMC[18,19] results for V3G tests with model at zero incidence: a) drag coefficient and b) overall heat transfer coefficient.

V3G Results

An experimental test program[7] has also been conducted for the 70-deg blunted cone with the V3G freejet facility of the DLR Göttingen. Drag, lift, global heat transfer, and recovery temperature were measured in a Mach 9 nitrogen freejet flow. These measurements were made for various degrees of rarefaction by including most of the transitional regime ($0.03 < Kn_0 < 6$) for stagnation temperatures of 295 and 500 K. The wall-to-stagnation temperature ratio was varied between 0.8–1.5. The copper model with a base diameter of 5 mm was suspended with a thermocouple at incident angles of 0, 20, and 40 deg. Details concerning the experiments, data reduction, data accuracy, and results are included in Ref. 3.

Results for T_0 = 300 K, T_w/T_0 = 1.0 and zero incidence are presented in Figs. 6a and 6b for the drag and overall heat transfer coefficient ($\overline{C_H} = 2Q/\rho_\infty V_\infty^3 A$), respectively. The overall accuracy of the experiments was estimated[3] to be ±8% for these conditions. The DSMC solutions of Refs. 18 and 19 are in very good agreement with the experimental results.

V2G Results

The vacuum wind-tunnel V2G at DLR, Göttingen, has been used extensively to support the blunt body/wake research. Both qualitative and quantitative data have been reported in Refs. 5–7 for models with and without a sting. The experiments were conducted in rarefied nitrogen flow at a nominal Mach number of 16 (see Table 1). Calibration results for the 15-deg half-angle conical nozzle used to produce the flow is reported in Ref. 4. Reference 6 details much of the qualitative results obtained for 50- and 25-mm base diameter models with and without (wire suspension) stings. The data includes high-frequency glow discharge flow visualization showing the shock shape, oil flow pictures giving surface streamlines, liquid crystal surface temperature visualization providing lines of constant temperature (lines of constant heat transfer under certain restrictions), and pitot pressure measurements in the wake. Data obtained with a 5-mm base diameter model is included in Ref. 7.

Reference 6 and 8 describe the experiments conducted in V2G utilizing the Patterson probe to extract molecular flux information within the wake as a function of location and view direction. The 5-cm base diameter models suspended at zero incidence by three tungsten wires of 0.1 mm diameter were used in this study. The measurements show that a vortex is established for the most rarefied case (case 1) and increases in length with decreasing Knudsen number. This is consistent with the DSMC calculated vortices included in Appendix A of Ref. 5. Figure 7 presents calculated and measured results for test case 2 (P_0 = 5 bar), and illustrates good agreement for the wake centerline number flux *nu*, ratioed to the freestream flux $(nV)_\infty$. The agreement is good in terms of both the extent of separation and the magnitude of the molecular fluxes. A more extensive presentation of the features of the wake flow, including the non-Maxwellian behavior of the distribution function for these test conditions, is given in Ref. 8 where DSMC calculations are compared with the measurements.

HEG Results

A series of experiments has been conducted in the HEG at the DLR, Göttingen, with a 70-deg spherically blunted cone having a base diameter of 15.24 cm. These tests have contributed to the high-enthalpy, higher Reynolds number portion of the WG 18 activity. Reference 7 describes several tests that have been conducted in air with enthalpies of 10–23 MJ/kg

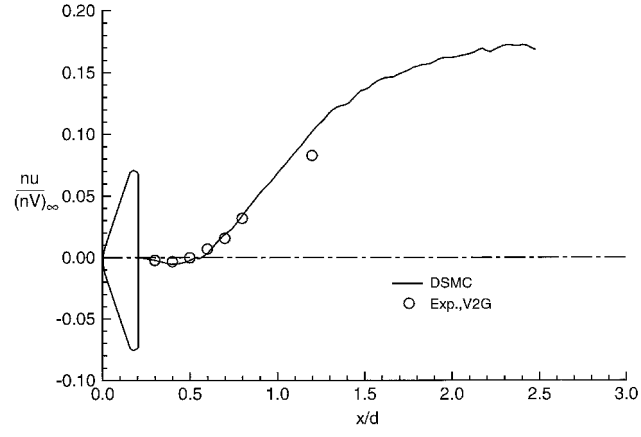

Fig. 7 Measured[2] and calculated[17] number flux along centerline of near wake for V2G test case 2.

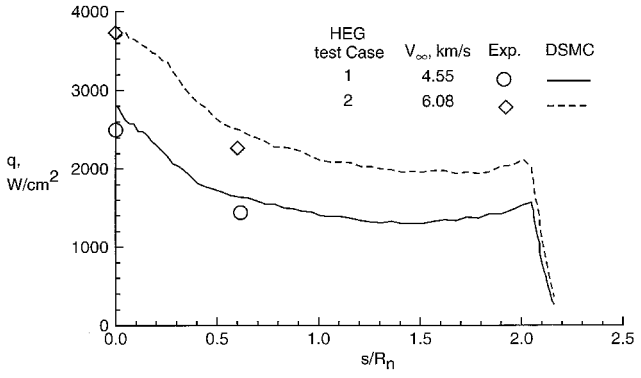

Fig. 8 Measured[7–9] and calculated[17] heating rates for two HEG tests using 5-mm base diameter models.

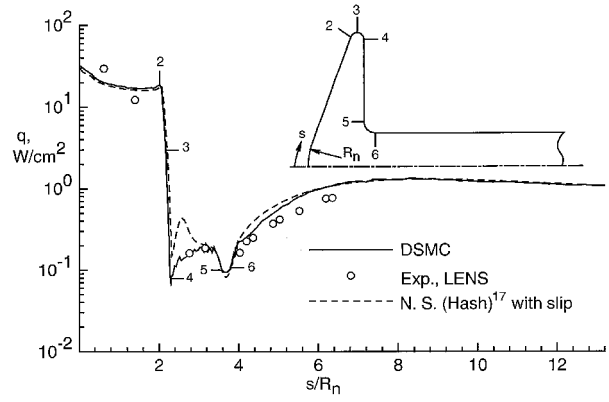

Fig. 9 Measured[10] and calculated[15,17] heating rate distributions for LENS test case 1.

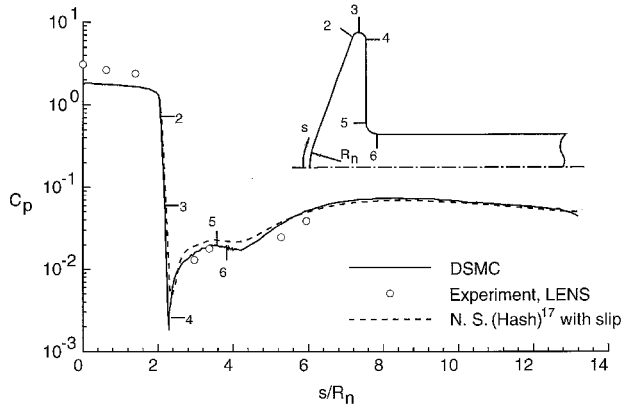

Fig. 10 Measured[10] and calculated[15,17] pressure distributions for LENS test case 1.

at freestream Mach numbers of approximately 10. For some of these tests, an array of four small models, 5 mm in diameter, were tested simultaneously with the larger model. The small models were located off centerline of the nozzle axis, as was the large model. Objectives of the small model tests were to assess different heating rate measurement techniques as well as to obtain heating rate data at two locations along the forebody. Details concerning the experiments, models, and data reduction are given in Refs. 7 and 9. The estimated error of the heat transfer measurements for the small cone tests is ±25%.[7] The scatter as shown in Ref. 7 is within ±20%.

Reference 7 presents the freestream conditions including the freestream gas composition as calculated with a one-dimensional nonequilibrium nozzle code for nine test conditions. Table 1 lists the freestream conditions for two of these tests [shots 132 (case 1), and 131 (case 2)] for which DSMC calculations[17] have been made. The DSMC calculations were made using a five-species reacting air gas model. For the lower enthalpy condition (case 1), the maximum mole fraction of atomic nitrogen behind the bow shock was of the order of 0.01, whereas the value for case 2 was of the order of 0.2. The calculated heating rate distributions for both cases are presented in Fig. 8 where the surface is assumed to be noncatalytic at a cold wall temperature of 300 K. Also shown are the measured results[7] at the stagnation point and an s/R_n location of 0.6. Good agreement is obtained for both shots concerning the distributions and absolute values.

LENS Results

As with the HEG experiments, several series of experiments have been conducted at Calspan with the large (d = 15.24 cm) blunted cone models. Tests have been made in the LENS facility using both nitrogen and air as test gases. Tests at both 5 and 10 MJ/kg conditions have been completed. Measurements consist of surface pressure and heating rates along the forebody, base, and sting. The focus of these tests are at continuum conditions; however, one test has been made at lower pressure conditions where rarefaction effects should be evident in the wake. The specifics of this test condition are listed in Table 1. Results of the experimental measurements for the low-pressure test were presented in Ref. 10, and DSMC results for this test condition have been reported in Refs. 10, 11, 15, and 17. Figures 9 and 10 present comparisons of calculated surface quantities for heating rate and pressure. The current DSMC results are compared with predictions obtained by Hash (see Ref. 17) using an implicit, three-temperature Navier–Stokes solver having the features discussed in Refs. 35 and 36. The slip boundary conditions used are those discussed in Ref. 37. The overall agreement between the DSMC and Navier–Stokes calculations is shown to be good, particularly along the sting. Largest differences occur along the base plane. The implication of the present comparison is that a Navier–Stokes solver can provide an adequate prediction of surface quantities for the current test problem.

Also shown in Figs. 9 and 10 are comparisons of measured and calculated values. As evident, there is good agreement between the calculations and measurements, both in the separated region and toward the end of the recompression process, indicating[10] that the size of the base flow region is well predicted. The agreement between the calculations and measurements along the forebody are not as good. The experimental pressure values are anomalously high (yielding a stagnation pressure coefficient of C_p = 3.0) and should be disregarded since the range of the pressure sensors were not appropriate along the forebody for this test. With only two heat transfer measurements along the forebody, it is not possible to establish the experimental trend for the heat transfer distribution.

Code-to-Code Predictions for Generic Flight Conditions

The flight-test cases consist of four individual cases to provide code-to-code comparisons for a 70-deg spherically blunted cone with a 2-m base diameter. No experimental results are available for these test cases. The test cases are for both Earth and Mars entry using both reacting and nonreacting gas models. The freestream and surface boundary conditions are specified in Ref. 1 and are listed in Table 2. These conditions correspond to altitudes of approximately 85 and 68 km in the Earth and Mars atmospheres, respectively. Results for Earth entry conditions have been reported in Refs. 24–26, whereas those for the Mars test case are presented herein by the present authors. In addition, Ref. 27 has presented results for conditions similar to the Mars test case, the only difference being that the freestream number density is 72.7% of the test case value and the wake is not included. Findings from these computational studies follow.

Table 2 Flight-test conditions[a]

Quantity	Earth entry	Mars entry
Number density, m^{-3}	1.654×10^{20}	1.654×10^{20}
Temperature, K	180.65	141
Velocity, km/s	7.0	7.0
Mole fraction N_2	0.7628	0.05
Mole fraction O_2	0.2372	——
Mole fraction CO_2	——	0.95

[a]70-deg spherically blunted cone with base diameter of 2 m and a noncatalytic surface with a wall temperature of 1000 K.

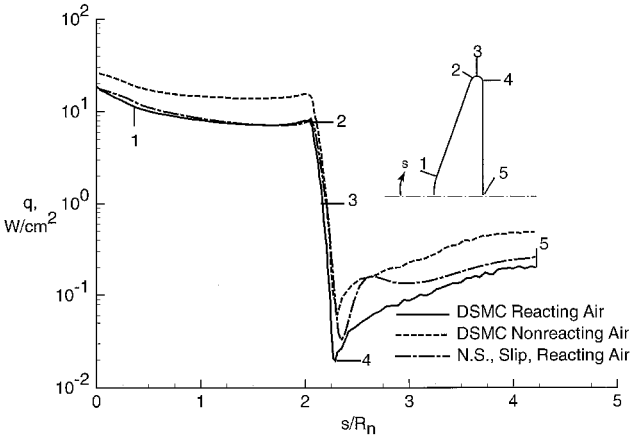

Fig. 11 Calculated[24] heating rate distributions for Earth entry (Alt = 85 km, V_∞ = 7.0 km/s, d = 2.0 m).

Reference 24 presented results for both the reacting and nonreacting air test cases calculated with the DSMC method and also reacting air solutions using an axisymmetric three-temperature, five-species implicit Navier–Stokes solver.[35,36] The DSMC and Navier–Stokes results[24] were in close agreement for the wake flowfield quantities. Also, the size of the vortex, as measured from the base of the blunted cone to the wake stagnation point, is identical for the two solutions.[24] However, there are some noticeable differences in the chemical composition within the wake. The most significant difference between the two solutions is in the surface heating calculations along the base plane (Fig. 11). The Navier–Stokes results for a reacting air model are 25–200% greater than the DSMC results for a reacting air model, while good agreement exists along the forebody. When the calculation is made for nonreacting air, as was done in Ref. 24, the results compared with the reacting air solution shows much higher surface heating rates, particularly along the base plane (240% higher); a smaller vortex; similar values for the wake density contours; and essentially the same value for drag.

DSMC solutions along the forebody are also included in Ref. 26 for this test case, where a different chemical reaction model is used compared to that of Ref. 24. Reacting and nonreacting results are presented showing the effect of the chemistry on stagnation temperature and density profiles, but not on heating rates. The reacting heating rate results are somewhat higher, particularly in the stagnation region, when compared to that of Ref. 24. Comparison of the nonreacting heating results for these two different solutions would be useful.

For Mars entry conditions, Ref. 27 presents forebody solutions with and without chemical reactions for the CO_2 and N_2 freestream gas mixture (Table 2). However, the heating results of Ref. 27 appear excessively high for both the nonreacting and nonequilibrium reacting flow cases based on engineering correlations, such as those given by Sutton and Graves[38] and reacting viscous-shock-layer (VSL) computation using the analysis of Gupta et al.[39] Figure 12 presents the heating distributions obtained with the DSMC method of Bird[40] for both the nonreacting and nonequilibrium reacting Mars test cases.

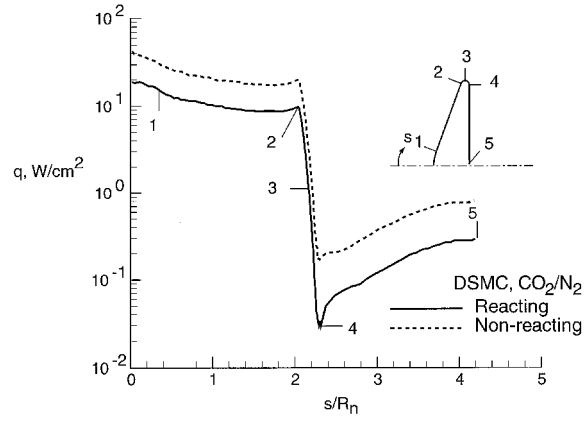

Fig. 12 Calculated heating rate distributions for Mars entry (Alt = 68 km, V_∞ = 7.0 km/s, d = 2.0 m).

The present results for the stagnation-point heating are in much better agreement with the aforementioned correlation and VSL results. Furthermore, the present heating values are a factor of 2 or more less than the calculated values in Ref. 27. The impact of the nonequilibrium chemical reactions on surface heating are similar to that for the Earth entry case, a significant reduction in heating for the noncatalytic wall assumption.

Additional calculations are needed for the generic flight-test cases, particularly the Mars test case, to assess the differences among solution methods as well as the modeling issues associated with nonequilibrium chemistry. Solutions with and without chemical reactions helps to isolate differences that might exist among solutions. A critical discriminator is the surface heating.

Comparison of DSMC Predictions to OREX Flight Data

A major benefit of combined experimental/computational studies is often the sanity check one provides the other. A goal of the computational effort is to demonstrate capability for various test cases to enhance the credibility of calculations for actual flight conditions. This section will comment on recent applications of one of the DSMC codes[40] that has been applied to several of the previously discussed test cases to a flight experiment. This was the OREX vehicle that was a 50-deg half-angle, spherically blunted cone with a base diameter of 3.4 m, a nose radius of 1.35 m, and a shoulder corner radius of 0.1 m.

OREX was flown in February of 1994, and initial results from this experiment are discussed in Refs. 28–30. The authors are not aware of any base heating or wake flow measurements made for the OREX.

Results of DSMC calculations that span the transitional flow regime (200–80 km) are presented in Refs. 31 and 32 where comparisons are made with flight inferred data and continuum calculations. Comparisons of DSMC results with OREX results were made for acceleration, surface pressure, and stagnation-point heating rates. In general, the comparisons show good agreement. For acceleration, the agreement is good (Fig. 13). The surface pressure data are in qualitative agreement (see Ref. 33). Calculated and measured surface pressure values are in good quantitative agreement for the lower altitudes, but diverge with increasing altitudes, as they should, because of the high degree of nonequilibrium that exists at and within the orifice inlet system used for the measured pressures. This is a situation where the inlet measured pressure can be substantially less than the surface pressure.

Agreement for calculated and measured stagnation-point heating rates is fair. Figure 14 presents the flight-inferred stagnation-point heating rate results as a function of time from launch of OREX. Continuum results obtained with VSL[31] and Navier–Stokes[30] solutions are shown for altitudes of 105–48.4 km. The NS results were for a no-slip and a noncatalytic sur-

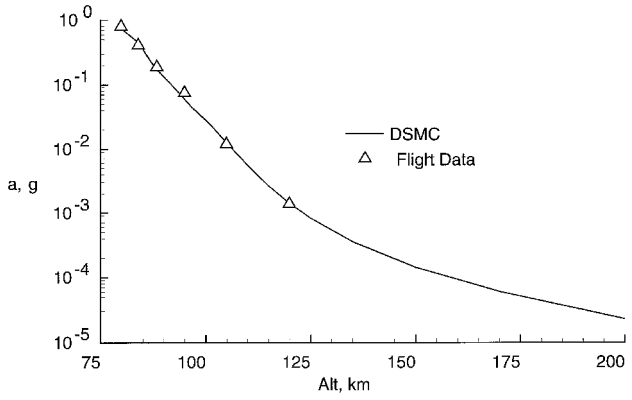

Fig. 13 Comparison of calculated[32] and measured[29] OREX axial acceleration.

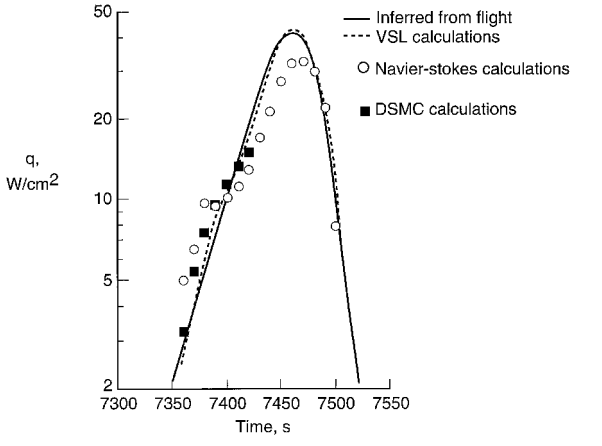

Fig. 14 Comparison of flight-inferred[30] stagnation-point heating rates for OREX with calculations using VSL,[31] NS,[30] and DSMC.[31]

face, which leads to much of the difference shown between the NS and flight results. The DSMC results shown for 105–79.9 km included the finite catalytic wall boundary conditions used in the VSL calculations; however, the finite catalytic and noncatalytic boundary conditions yield essentially the same results over this altitude range (see Ref. 31). For altitudes less than 80 km, the VSL results of Ref. 31 show that a finite catalytic surface boundary condition produces improved agreement with the flight results compared to the noncatalytic assumption. Inclusion of slip boundary conditions at the higher altitudes yields substantially lower heating rates for a continuum solution, as is discussed in Ref. 31. The heating rates are inferred from the temperature measurements made on the back surface of a carbon–carbon material. As additional data are reported, opportunities will exist for comparing calculated and measured results at various locations along the forebody. The overall good correspondence of flight and calculated results is encouraging.

Concluding Remarks

A review of recent experimental and computational studies focused on blunt body forebody and wake flows is presented where the emphasis is on rarefied flows. An objective of this AGARD Fluid Dynamics Working Group 18 problem was to determine how the near-wake structure is influenced by rarefaction and real-gas effects. The approach to achieve this objective was to select a generic blunt body configuration (70-deg spherically blunted cone) and encourage experimental contributions from the AGARD community. Once the experimental conditions were defined or conducted, computational contributions were solicited for the various experiments along with two generic flight conditions for entry into the atmosphere of Earth and Mars.

A key aspect of the success of this activity has been the experimental contributions from five hypersonic facilities that have fostered a significant number of computational contributions. Even with the estimated measurement uncertainties being large in some cases, the synergy of the computational/experimental activities has produced a significant database that can serve as a valuable aid for aerobraking mission designs. Some of the key contributions or findings of this activity are 1) first experimental measurements of density field and number flux for a generic Aeroassist Space Transfer Vehicle configuration; 2) database involving both quantitative and qualitative information that spans a wide range of conditions (nonreacting to reacting flows) in the transitional regime; 3) demonstrated capability of different DSMC codes to simulate selected test cases (SR3, condition 2); 4) the experimental (V2G, Patterson probe) and computational findings that show that a vortex is established when there is a strong non-Maxwellian distribution function in the wake and the size of the wake vortex increases with decreasing Knudsen number; 5) the maximum heating along a sting/afterbody for zero incidence was of the order of 5% of the forebody stagnation value; 6) the location of wake reattachment and maximum sting heating rate are not coincident, and the separation between the two locations diminishes with decreasing rarefaction; 7) inclusion of slip boundary conditions in the Navier–Stokes solvers provided improved agreement with experimental and DSMC results; 8) results from the Navier–Stokes solutions suggest that the overall Knudsen number should be of the order of 0.001 or less before good agreement is achieved between experiment or DSMC for the near-wake surface and flow features, and that the Navier–Stokes solutions agree with the DSMC results for quite large overall Knudsen numbers along the forebody; and 9) for the generic flight-test cases that involve substantial dissociation, the calculated forebody and afterbody heating for the reacting solutions are substantially less than for the corresponding nonreacting cases.

Readily evident from the previous findings and the comparisons with the OREX flight measurements is a demonstrated capability of the DSMC method to calculate complex flow features including surface heating to good accuracy when compared to experimental measurements, both ground based and flight.

References

[1]Anon., "Hypersonic Experimental and Computational Capabilities: Improvement and Validation," AGARD AR-319, Vol. 1, May 1996.

[2]Allegre, J., and Bisch, D., "Blunted Cone at Rarefied Hypersonic Conditions—Experimental Density Flowfields, Heating Rates, and Aerodynamic Forces," CNRS Rept., RC 95-2, Sept. 1995.

[3]Legge, H., "Heat Transfer and Forces on a Blunted 70 Deg. Half Angle Cone Measured in Hypersonic Free Jet Flow," DLR Rept., IB 222-93 A 33, Nov. 1993.

[4]Legge, H., Von Roden, G., Klotzbach, A., and Rammenzwieg, D., "Calibration Data of V2G with a Conical Ma ≈ 15 Nozzle," DLR, IB 223-94 A 11, March 1994.

[5]Legge, H., "Patterson Probe Measurements in the Wake of a 70 Deg. Half Angle Cone in Hypersonic Rarefied Flow," DLR Rept., IB 223-94 A 15, Dec. 1994.

[6]Legge, H., "Flow Visualization and Pitot Probe Measurements in Hypersonic Rarefied Flow Around a 70 Deg. Half Angle Cone," DLR Rept., IB 223-95 A 01, Feb. 1995.

[7]Legge, H., "Experiments on a 70 Degree Blunted Cone in Rarefied Hypersonic Wind Tunnel Flow," AIAA Paper 95-2140, June 1995.

[8]Danckert, A., and Legge, H., "Experimental and Computational Wake Structure Study for a Wide-Angle Cone," *Journal of Spacecraft and Rockets*, Vol. 33, No. 4, 1996, pp. 476–482; also AIAA Paper 95-2141, June 1995.

[9]Legge, H., Rammenzweig, D., and Klotzbach, A., "Heat Transfer Measurements on a Blunted 70 Deg Half Angle Cone in High Enthalpy Small Reynolds Number Flow," DLR Rept., IB 223-95 A 22, March 1996.

[10]Holden, M., Kolly, J., and Chadwick, K., "Calibration, Validation, and Evaluation Studies in the LENS Facility," AIAA Paper 95-0291, 1995.

[11]Holden, M. S., Chadwick, K. M., Gallis, M. A., and Harvey, J. K., "Comparison Between Shock Tunnel Measurements on a Planetary Probe Configuration and DSMC Predictions," 20th ISSW, California Inst. of Technology, Pasadena, CA, July 1995.

[12]Moss, J. N., Mitcheltree, R. A., Dogra, V. K., and Wilmoth, R. G., "Direct Simulation Monte Carlo and Navier–Stokes Simulations of Blunt Body Wake Flows," *AIAA Journal*, Vol. 32, No. 7, 1994, pp. 1399–1406; also AIAA Paper 93-2807, July 1993.

[13]Wilmoth, R. G., Mitcheltree, R. A., Moss, J. N., and Dogra, V. K., "Zonally Decoupled Direct Simulation Monte Carlo Solutions of Hypersonic Blunt-Body Wake Flows," *Journal of Spacecraft and Rockets*, Vol. 31, No. 6, 1994, pp. 971–979; also AIAA Paper 93-2808, July 1993.

[14]Moss, J. N., Dogra, V. K., and Wilmoth, R. G., "DSMC Simulations of Mach 20 Nitrogen Flows About a 70° Blunted Cone and Its Wake," NASA TM-107762, Aug. 1993.

[15]Moss, J. N., Price, J. M., and Dogra, V. K., "DSMC Calculations for a 70° Blunted Cone at 3.2 km/s in Nitrogen," NASA TM-109181, Jan. 1995.

[16]Dogra, V. K., Moss, J. N., Taylor, J. C., Hash, D. B., and Hassan, H. A., "Rarefaction Effects on Blunt-Body Wake Structure," *Rarefied Gas Dynamics 19*, edited by J. Harvey and G. Lord, Oxford Univ. Press, Oxford, England, UK, 1995, pp. 1154–1160.

[17]Moss, J. N., Dogra, V. K., Price, J. M., and Hash, D. B., "Comparison of DSMC and Experimental Results for Hypersonic External Flows," AIAA Paper 95-2028, June 1995.

[18]Gallis, M. A., and Harvey, J. K., "Comparison of the Maximum Entropy DSMC Code with Flowfield Measurements," AIAA Paper 95-0413, Jan. 1995.

[19]Gallis, M. A., and Harvey, J. K., "Validation of DSMC Computations for the Flowfield Around a 70° Blunted Cone," *Rarefied Gas Dynamics 19*, edited by J. Harvey and G. Lord, Oxford Univ. Press, Oxford, England, UK, 1995, pp. 1284–1290.

[20]Marriott, R. M., and Bartel, T. J., "Comparison of DSMC Flow Field Predictions Using Different Models for Energy Exchange and Chemical Reaction Probability," *Rarefied Gas Dynamics 19*, edited by J. Harvey and G. Lord, Oxford Univ. Press, Oxford, England, UK, 1995, pp. 413–419.

[21]Gilmore, M. R., "Rarefied Flow over a Blunt Body," Defence Research Agency, DWS/WX7/TR 95 189, Feb. 1995.

[22]Coron, F., and Harvey, J. K., "Synopsis for Test Case 6—Rarefied 70° Spherically Blunted Cone," 4th European High-Velocity Database Workshop, ESTEC, Noordwijk, The Netherlands, Nov. 1994.

[23]Pallegoix, J. F., "Workshop ESTEC—Test Case No. 6—Rarefied Spherically Blunted Cone," 4th European High-Velocity Database Workshop, ESTEC, Noordwijk, The Netherlands, Nov. 1994.

[24]Dogra, V. K., Moss, J. N., Wilmoth, R. G., Taylor, J. C., and Hassan, H. A., "Effects of Chemistry on Blunt-Body Wake Structure," *AIAA Journal*, Vol. 33, No. 3, 1995, pp. 463–469; also AIAA Paper 94-0352, Jan. 1994.

[25]Dogra, V. K., Moss, J. N., Wilmoth, R. G., Taylor, J. C., and Hassan, H. A., "Blunt Body Rarefied Wakes for Earth Entry," *Journal of Thermophysics and Heat Transfer*, Vol. 9, No. 3, 1995, pp. 464–470; also AIAA Paper 93-0271, Jan. 1993.

[26]Gallis, M. A., and Harvey, J. K., "Implementation of a Maximum Entropy Method in Monte Carlo Direct Simulations," AIAA Paper 95-2094, June 1995.

[27]Gallis, M. A., and Harvey, J. K., "Analysis of Non-Equilibrium in Mars Atmosphere Entry Flows," AIAA Paper 95-2095, June 1995.

[28]NAL/NASDA Joint Research Rept., OREX, March 1995 (in Japanese).

[29]Inouye, Y., "OREX Flight—Quick Report and Lessons Learned," 2nd European Symposium on Aerothermodynamics of Space Vehicles, Invited Paper 4, ESTEC, Nov. 1994.

[30]Yamamoto, Y., and Yoshioka, M., "CFD and FEM Coupling Analysis of OREX Aerothermodynamic Flight Data," AIAA Paper 95-2087, June 1995.

[31]Gupta, R. N., Moss, J. N., and Price, J. M., "Assessment of Thermochemical Nonequilibrium and Slip Effects for Orbital Reentry Experiment (OREX)," AIAA Paper 96-1859, June 1996.

[32]Moss, J. N., Gupta, R. N., and Price, J. M., "DSMC Simulations of OREX Entry Conditions," 20th International Symposium on Rarefied Gas Dynamics, Beijing, China, Aug. 1996.

[33]Gnoffo, P. A., "An Upwind-Biased, Point-Implicit Relaxation Algorithm for Viscous Compressible Perfect-Gas Flows," NASA TP-2953, Feb. 1990.

[34]Gnoffo, P. A., Gupta, R. N., and Shinn, J. L., "Conservation Equations and Physical Models for Hypersonic Air Flows in Thermal and Chemical Nonequilibrium," NASA TP-2867, Feb. 1989.

[35]Olynick, D. R., and Hassan, H. A., "New Two-Temperature Dissociation Model for Reacting Flows," *Journal of Thermophysics and Heat Transfer*, Vol. 7, No. 4, 1993, pp. 687–696.

[36]Olynick, D. R., Taylor, J. C., and Hassan, H. A., "Comparisons Between DSMC and the Navier-Stokes Equations for Reentry Flows," AIAA Paper 93-2810, July 1993.

[37]Gupta, R. N., Scott, C. D., and Moss, J. N., "Slip-Boundary Equations for Multicomponent Nonequilibrium Airflow," NASA TP-2452, Nov. 1985.

[38]Sutton, K., and Graves, R. A., "A General Stagnation-Point Convective-Heating Equation for Arbitrary Gas Mixtures," NASA TR-376, Nov. 1971.

[39]Gupta, R. N., Lee, K. P., and Scott, C. D., "Aerothermal Study of Mars Pathfinder Aeroshell," *Journal of Spacecraft and Rockets*, Vol. 33, No. 1, 1996, pp. 61–69.

[40]Bird, G. A., *Molecular Gas Dynamics and the Direct Simulation of Gas Flows*, Clarendon, Oxford, England, UK, 1994.